arXiv:1002.1669v1 [nucl-ex] 8 Feb 2010

The proton and deuteron F_2 structure function at low Q^2

V. Tvaskis,[1,2,3] J. Arrington,[4] R. Asaturyan,[5] O. K. Baker,[3] H. P. Blok,[1,2] P. Bosted,[6] M. Boswell,[7] A. Bruell,[8] M. E. Christy,[3] A. Cochran,[3] R. Ent,[6] B. W. Filippone,[9] A. Gasparian,[3] C. E. Keppel,[3,6] E. Kinney,[10] L. Lapikás,[2] W. Lorenzon,[11] D. J. Mack,[6] J. Mammei,[12] J. W. Martin,[8] H. Mkrtchyan,[5] I. Niculescu,[13] R. B. Piercey,[14] D.H. Potterveld,[4] G. Smith,[6] K. Spurlock,[14] G. van der Steenhoven,[2] S. Stepanyan,[5] V. Tadevosian,[5] and S. A. Wood[6]

[1] *VU University, 1081 HV Amsterdam, The Netherlands*
[2] *National Institute for Subatomic Physics (Nikhef), 1009 DB Amsterdam, The Netherlands*
[3] *Hampton University, Hampton, Virginia 23668*
[4] *Argonne National Laboratory, Argonne, Illinois 60439*
[5] *Yerevan Physics Institute, 375036, Yerevan, Armenia*
[6] *Thomas Jefferson National Accelerator Facility, Newport News, Virginia 23606*
[7] *Randolph-Macon Woman's College, Lynchburg, Virginia 24503*
[8] *Massachusetts Institute of Technology, Cambridge, Massachusetts 02139*
[9] *California Institute of Technology, Pasadena, California 91125*
[10] *University of Colorado, Boulder, Colorado 80309*
[11] *University of Michigan, Ann Arbor, Michigan 48109*
[12] *Juniata College, Huntingdon, Pennsylvania 16652*
[13] *The George Washington University, Washington, D.C. 20052*
[14] *Mississippi State University, Mississippi State, Mississippi 39762*

(Dated: February 8, 2010)

Measurements of the proton and deuteron F_2 structure functions are presented. The data, taken at Jefferson Lab Hall C, span the four-momentum transfer range $0.06 < Q^2 < 2.8$ GeV^2, and Bjorken x values from 0.009 to 0.45, thus extending the knowledge of F_2 to low values of Q^2 at low x. Next-to-next-to-leading order calculations using recent parton distribution functions start to deviate from the data for $Q^2 < 2$ GeV^2 at the low and high x-values. Down to the lowest value of Q^2, the structure function is in good agreement with a parameterization of F_2 based on data that have been taken at much higher values of Q^2 or much lower values of x, and which is constrained by data at the photon point. The ratio of the deuteron and proton structure functions at low x remains well described by a logarithmic dependence on Q^2 at low Q^2.

PACS numbers: 13.60.-r,12.38.Qk,13.90.+i,13.60.Hb

Deep-inelastic scattering (DIS) remains a powerful tool to study the partonic substructure of the nucleon. Decades of experiments with high-energy electron and muon beams have provided a detailed map of the nucleon structure function $F_2(x, Q^2)$ over many orders of magnitude in x and Q^2 [1]. Here, Q^2 is the negative square of the four-momentum transfer of the virtual photon exchanged in the scattering process, and $x = Q^2/2M\nu$ is the Bjorken scaling variable, with M the nucleon mass and ν the energy of the virtual photon in the target rest frame. In the region of large Q^2 and ν, the results of these DIS measurements are typically interpreted in terms of partons (quarks and gluons), where x can be interpreted as the fraction of the nucleon momentum carried by the struck parton.

In this regime, a rigorous theoretical framework is provided by perturbative Quantum Chromodynamics (pQCD), which gives logarithmic scaling violations in Q^2 [2]. However, this description starts to fail when non-perturbative effects such as interactions between the quark struck in the scattering process and other quarks or gluons in the nucleon become important. The sensitivity for such higher-twist effects increases with decreasing Q^2, since they are proportional to powers of $1/Q^2$. Therefore, the interpretation of the nucleon structure functions in terms of partons was originally anticipated to become suspect when momentum and energy transfers get below a few GeV. Nonetheless, the perturbative descriptions were shown to hold down to surprisingly low values of Q^2, of the order of 1 GeV^2, provided that the energy transfer remained sufficiently large [3].

For small values of the energy transfer, corresponding to an invariant mass $W = \sqrt{M^2 + 2M\nu - Q^2} < 2$ GeV of the hadronic system, the data at low Q^2 prominently show excitation of nucleon resonances, and a simple partonic interpretation fails. Moving beyond this resonance region, the behaviour of the nucleon structure functions in the low Q^2 region is thought to shed light on the transition from perturbative to non-perturbative QCD within the partonic interpretation. However, little is known about this behaviour, since for $W > 2$ GeV there are few data points at low Q^2, except for the (transverse) cross section σ_T at exactly $Q^2 = 0$ from real-photon absorption experiments, some data from SLAC [4], and data at very low x values ($x < 0.005$) from the E665, ZEUS and H1 experiments [5–7]. Here, we report on measure-

ments in the range $0.009 < x < 0.45$, approaching the valence-quark region, for $0.06 < Q^2 < 2.8$ GeV^2.

The differential cross section for inclusive electron scattering can be written as

$$\frac{d^2\sigma}{d\Omega dE'} = \Gamma_v(\sigma_T + \varepsilon\sigma_L), \quad (1)$$

where the virtual-photon flux factor is given by

$$\Gamma_v = \frac{\alpha}{2\pi^2}\frac{E'}{E}\frac{K}{Q^2}\frac{1}{1-\varepsilon}, \quad (2)$$

with $K = (W^2 - M^2)/2M$, ε the virtual photon polarization, and σ_L (σ_T) the longitudinal (transverse) virtual-photon absorption cross section, which depends on x and Q^2. Usually, the cross section is written in terms of the structure functions $F_1(x, Q^2)$ and $F_2(x, Q^2)$, where F_1 is proportional to σ_T and F_2 is proportional to $\sigma_L + \sigma_T$. However, the cross section can also be written in terms of F_2 and the ratio $R \equiv \sigma_L/\sigma_T$ according to:

$$\frac{d^2\sigma}{d\Omega dE'} = \frac{4\pi^2\alpha}{1-x}\frac{1}{Q^2}(1 + \frac{4M^2x^2}{Q^2})\,F_2\,\frac{1+\varepsilon R}{1+R}. \quad (3)$$

This equation shows that in the limit $\varepsilon \to 1$, the structure function F_2 can directly be determined from the measured cross section. Otherwise, measurements have to be performed for at least two different values of ε (beam energies) at fixed values of x and Q^2 (Rosenbluth separation), or a value for R has to be assumed. Although results for the F_2 structure function have been widely reported [4–19], in many cases assumptions on the value of R were made. A more limited set of experiments actually performed Rosenbluth-separations [4, 8, 10–14]. In this paper we present results for F_2 based on data for both hydrogen and deuterium at low values of Q^2, utilizing both techniques: using Rosenbluth-separated data and using unseparated data in combination with a parametrization of $R(x, Q^2)$. Values of R extracted from these data for those kinematics, where data were taken at more than one value of ε, were reported previously [20]. Here the full data set is used to determine F_2.

The experiment (E99-118) was carried out in experimental Hall C at the Thomas Jefferson National Accelerator Facility (JLab). Data were obtained for $0.009 < x < 0.45$, $0.06 < Q^2 < 2.8$ GeV^2 by utilizing 2.301, 3.419 and 5.648 GeV electron beams at a current of $I = 25\,\mu$A. The minimum scattered electron energy was $E' \approx 0.4$ GeV and the range of the invariant mass of the hadronic system W was between 1.9 and 3.2 GeV^2. Electrons scattered from 4 cm long liquid hydrogen and deuterium targets were detected in the High-Momentum Spectrometer (HMS) in Hall C at various angles between 10° and 60°.

The inclusive double differential cross section for each energy and angle bin within the spectrometer acceptance was determined from the measured electron yields. The yields were corrected for detector inefficiencies, background events, and finally radiative effects to obtain the Born cross section. Internal bremsstrahlung, vertex corrections and loop diagrams were calculated using the approach by Bardin *et al.* [21]. The code used includes the possibility that the electron emits two hard photons (α^2 term). However, the calculation of this process is not yet fully established. Because the calculation including the α^2 term overestimates the radiative tail, perhaps because higher-order terms associated with the emission of more than two hard photons are not negligible, only half of the two hard-photon correction was applied, and the size of the correction was included in the cross section systematic uncertainty (see Ref. [22] for more details). Additional radiative effects in the target and its exit windows were determined using the formalism of Mo and Tsai [23].

For every bin the cross section was corrected for the variation of the cross section over the acceptance with the angle θ to yield the value of the cross section at the central angle (bin-centering correction). To minimize the dependence on the model used to describe this variation and the radiative effects, an iterative procedure was employed. A similar procedure was used to center the cross sections at chosen values of x. For details regarding the analysis and the standard Hall C apparatus employed in this experiment, see Refs. [20, 22, 24, 25].

The total uncertainty in the cross sections was calculated as the quadratic sum of statistical and systematic uncertainties. The statistical uncertainty was in most cases well below 1%. The systematic uncertainty on the cross sections from instrumental sources such as target thickness, charge integration, various efficiencies, and acceptance amounted to 1.3% - 1.7%. The uncertainty in the radiative corrections is about 1%, except at low values of E' ($E' < 0.8$ GeV), where the measured data are dominated by events from elastic or quasi-elastic scattering with the emission of one or more photons in the initial or final state. The estimate of these uncertainties was determined by varying all relevant input cross sections within their uncertainties, and amounted to 1.5% for hydrogen and 8.5% for deuterium in the most extreme cases considered. The much larger uncertainty in the deuterium cross section is due to the contribution from quasielastic scattering, which can only be modelled approximately due to the lack of low-Q^2 (< 0.4 GeV^2) electron-deuteron scattering data over a sufficiently wide range of energy transfers. In addition, there is the uncertainty from the α^2 term, which can be as large as 50% in a few cases (low values of x and ε).

The results for the $F_2(x, Q^2)$ structure function for protons (deuterons) from the Rosenbluth separated data are shown as the open squares in Fig. 1 (Fig. 2) as a function of Q^2 for fixed values of x. The value of F_2 and its uncertainty are in essence the result of an extrapolation of the cross sections and their (total) uncertainties, measured at the different ε values, to $\varepsilon = 1$ and were cal-

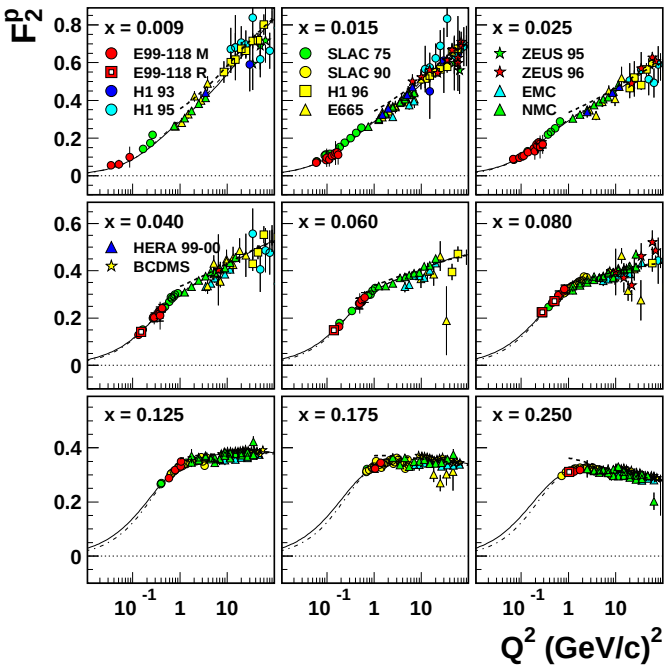

FIG. 1: Comparison of the results for $F_2^p(x, Q^2)$ from the present experiment (E99-118) to the results of other experiments. Both the Rosenbluth-separated data (open red squares) and the model-dependent extracted data (red circles) are shown. The thick dashed curve represents the result of a NNLO calculation based upon the MRST parton distributions [29] including target-mass effects. The solid and dot-dashed curves are the results of the phenomenological parameterizations from Refs. [31, 32], respectively.

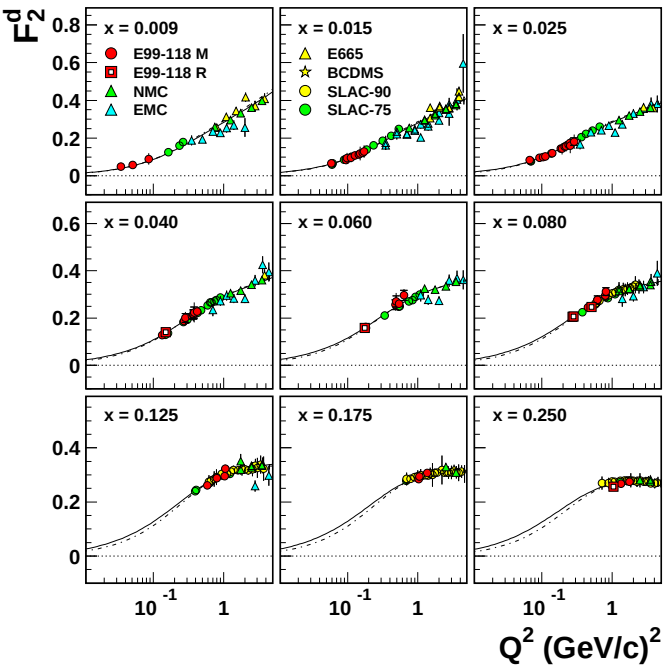

FIG. 2: Comparison of the results for $F_2^d(x, Q^2)$ from the present experiment (E99-118) to the results of other experiments. Both the Rosenbluth-separated data (open red squares) and the model-dependent extracted data (red circles) are shown. The solid and dot-dashed curves result from multiplying the phenomenological parameterizations shown in Fig. 1 with $(1 + F_2^n/F_2^p)/2$ using the NMC parameterization [27] for the ratio F_2^n/F_2^p.

culated accordingly. The numerical values [26] are given in Table I.

Values of F_2 from the unseparated data were determined by inverting Eq. 3 and using a recent parametrization of R. Measurements of $R(x, Q^2)$ from the present experiment reported in [20] showed a nearly constant behaviour of R down to Q^2 of about 0.1 GeV^2 at low values of x. This was contrary to expectations that R would decrease strongly at such low Q^2. The unexpected behaviour was taken into account by extending the parameterization of Ref. [4] to $Q^2 = 0$, resulting in a new $R_{e99118}(x, Q^2)$ parameterization [20]. This parameterization was used to calculate F_2 for all values of x and Q^2 where cross sections from the present experiment are available that were not used already for the Rosenbluth separation. The uncertainty in F_2 is a combination of the uncertainties in the measured cross section and in the parameterization of R. For $Q^2 > 1$ GeV^2 the latter uncertainty was taken to be 0.075 . For $Q^2 < 1$ GeV^2 the value of R is less well known, as there are few measurements in that region, especially at very small values of Q^2. Therefore, in this region an uncertainty increasing from 0.075 at $Q^2 = 1$ GeV^2 to 0.20 at $Q^2 = 0$ GeV^2 was taken. This gives a range for R that covers well the existing data in this region. The influence of R on the extracted value of F_2 diminishes when $\varepsilon \to 1$. The results are shown as the red circles in Figs. 1,2. They agree well with the Rosenbluth-separated results, but cover a much larger kinematic range. Also, there is a very good consistency between the results at the same value of x and almost the same value of Q^2, but different values of ε, as can be seen from the numerical values given in Table II.

Both figures also show the results of previous measurements at SLAC [4], by the EMC [13], NMC [14, 27, 28] and BCDMS [8, 9] collaborations at CERN, the E665 [5] collaboration at Fermilab, and the H1 [15–17] and ZEUS [18, 19] collaborations at DESY. In the region of Q^2 where these overlap with the present results there is good agreement. At low x our data clearly extend the knowledge of F_2 down to much lower Q^2.

The thick dashed curves shown in Fig. 1 are the result of a next-to-next-to-leading order (NNLO) calculation based on the recent MRST parton distributions [29], where target-mass effects have been included according to [30]. The calculations do not extend below $Q^2 = 1$ GeV^2, as there a DIS approach is not assumed to be applicable anymore. The calculated results closely coincide with the data for $x \approx 0.1$. Deviations can be noticed at the lower Q^2 end for the lowest ($x = 0.009$) and highest

($x = 0.250$) x-values. This could be due to uncertainties in the used parton distribution functions at low x and the influence of higher-twist effects.

The solid and dot-dashed curves shown in Fig. 1 represent two existing parameterizations down to the photon point of the world's F_2^p data, termed ALLM97 and GD07. The ALLM97 parameterization [31] represents a 23-parameter fit to world's electron-proton scattering total cross section data based upon a Regge-motivated approach. It includes both Reggeon and Pomeron exchange mechanisms. Deep-inelastic scattering data covering a wide range in x and Q^2 are used, with additional constraints built in to connect smoothly to the photon point. The GD07 parameterization [32] includes recent data and converts from total cross sections to F_2 structure functions by using the parameterization of R from Ref. [33] for all data.

The solid (dot-dashed) curves shown on Fig. 2 were constructed by utilizing the mentioned ALLM97 and GD07 parameterizations of F_2^p, multiplying them by the factor $(1 + F_2^n/F_2^p)/2$ using a global fit to F_2^n/F_2^p data by the NMC collaboration [27]. As can be seen from Figs. 1 and 2, the existing parameterizations are in very good agreement with the measured structure functions, with deviations often less than 3% and always consistent given the error bars. The largest deviations occur for data that have large systematic uncertainties. Given that for $x < 0.1$ there were no data for $Q^2 \lesssim 1$ GeV^2, the agreement between our data and the parameterizations is remarkable. This indicates that the constraints imposed on the parameterizations by low-Q^2 data at much smaller x and the way the transition to the real photon point at $Q^2 = 0$ is parametrized, seem to be sufficient to correctly predict $F_2(x, Q^2)$ in a region where it was hitherto unknown.

The ratio of the deuteron to proton structure functions, F_2^d/F_2^p is of interest because it embodies information on the neutron structure function F_2^n. This ratio can be expressed in terms of the cross section ratio σ^d/σ^p as

$$\frac{F_2^d}{F_2^p} = \left(\frac{\sigma^d}{\sigma^p}\right) \frac{(1 + \varepsilon R^p)(1 + R^d)}{(1 + R^p)(1 + \varepsilon R^d)} \ , \qquad (4)$$

with σ^d/σ^p the measured cross section ratio and R^d and R^p both functions of x and Q^2.

For sufficiently high energy experiments, $\varepsilon \to 1$, and the deuteron to proton cross section and F_2 ratios will equate. Similarly, the ratios equate if $R^p = R^d$, which has been found in all previous higher-Q^2 data, albeit with relatively large uncertainties, see Ref. [11, 27]. However, the data from the present experiment are at $\varepsilon \neq 1$ and, as reported earlier [20], there may be a small reduction of R^d with respect to R^p at low Q^2 ($Q^2 < 1.5$ GeV^2). Such a reduction was taken into account when converting our measured σ^d/σ^p ratios to F_2^d/F_2^p ratios. (The systematic error in the latter ratio includes the effect of an uncertainty in the value of $R_d - R_p$, which conservatively was taken equal to the value of $R_d - R_p$.) The effect is small, decreasing the extracted ratio F_2^d/F_2^p by up to a few percent as compared to the σ^d/σ^p ratio, depending on the value of ε and Q^2. Fig. 3 shows the present F_2^d/F_2^p data for selected x bins in comparison with the world's data. The numerical values of all present data are given in Table III.

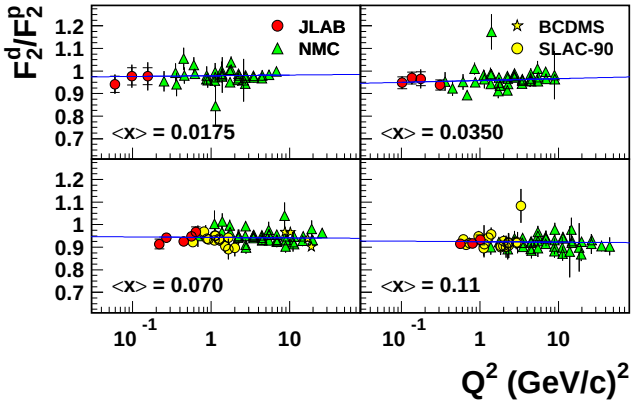

FIG. 3: Q^2 dependence of the ratio F_2^d/F_2^p for some selected x-bins. Both the present data and data from previous experiments are shown. The lines are the results of a linear (in $\ln Q^2$) fit of all data described in the text.

The precise data from the NMC collaboration [27] have shown that the F_2^d/F_2^p ratio depends (at fixed x) logarithmically on the scale, Q^2. The data from the present experiment extend the Q^2 range of the data in the region $0.01 < x < 0.1$, thus improving the knowledge of these logarithmic Q^2-dependences in that region. Neglecting differences in higher-twist effects in the proton and deuteron, all data for F_2^d/F_2^p were fitted with the linear function $\frac{F_2^d}{F_2^p}(x, Q^2) = A(x) + B(x) \ln(Q^2)$. The data for F_2^d/F_2^p from the present experiment are found to be in excellent agreement with this parameterization, see the lines in Fig. 3.

In summary, we present F_2 structure function data taken on hydrogen and deuterium spanning the four-momentum transfer range $0.06 < Q^2 < 2.8$ GeV^2. The data are at lower Q^2 values than hitherto reported in the range of small to intermediate x, $0.009 < x < 0.45$. The data agree well with the results of phenomenological parameterizations based upon data accumulated at either much larger Q^2, or far smaller values of x. Results of NNLO calculations agree with the data for $x \approx 0.1$, but deviate at lower and higher values of x, when Q^2 drops below 2 GeV^2. The present data extend the data set for the ratio of deuteron to proton F_2 structure functions to

TABLE I: Data for the proton and deuteron F_2 structure function as determined via the Rosenbluth separation method. Uncertainties are shown without (Δ_{norc}) and with (Δ_{full}) the contribution from radiative corrections.

x	Q^2	F_2^p	Δ^p_{norc}	Δ^p_{full}	F_2^d	Δ^d_{norc}	Δ^d_{full}
0.040	0.150	0.1407	0.0035	0.0046	0.1405	0.0036	0.0046
0.060	0.145	0.1477	0.0033	0.0053	0.1579	0.0034	0.0042
0.080	0.273	0.2238	0.0039	0.0053	0.2045	0.0039	0.0044
0.080	0.283	0.2250	0.0041	0.0054	0.2068	0.0038	0.0043
0.080	0.508	0.2715	0.0046	0.0074	0.2470	0.0042	0.0058
0.175	0.476	0.2753	0.0060	0.0062	0.2438	0.0119	0.0121
0.250	1.045	0.3103	0.0054	0.0057	0.2565	0.0042	0.0045
0.350	1.300	0.2674	0.0035	0.0036	0.2274	0.0051	0.0052
0.350	1.670	0.2648	0.0046	0.0046	0.2140	0.0033	0.0038

lower Q^2. The new data are in excellent agreement with higher-Q^2 data, when the logarithmic dependence on Q^2 is taken into account.

This work is supported in part by research grants from the U.S. Department of Energy, the U.S. National Science Foundation, and the Stichting voor Fundamenteel Onderzoek der Materie (FOM) of the Netherlands. The Southeastern Universities Research Association operates the Thomas Jefferson National Accelerator Facility under the U.S. Department of Energy contract DEAC05-84ER40150.

[1] Particle Data Group, Phys. Lett. **B667**, 1 (2008).
[2] R. P. Feynman, *Photo-Hadron Interactions*, W. A. Benjamin Inc. Reading, MA (1976).
[3] M. Gluck, E. Reya, A. Vogt, Z. Phys. **C67**, 433 (1995).
[4] L. W. Whitlow *et al.*, Phys. Lett. **B250**, 193 (1990) and references therein.
[5] M. R. Adams *et al.*, Phys. Rev. D **54**, 3006 (1996).
[6] M. Breitweg *et al.*, Phys. Lett. **B487**, 53 (2000).
[7] C. Adloff *et al.*, Nucl. Phys. **B497**, 3 (1997).
[8] A. C. Benvenuti *et al.*, Phys. Lett. **B223**, 485 (1989).
[9] A. C. Benvenuti *et al.*, Phys. Lett. **B237**, 592 (1990).
[10] S. Dasu *et al.*, Phys. Rev. Lett. **60**, 2591 (1988).
[11] L. H. Tao *et al.*, Z. Phys. **C70**, 387 (1996).
[12] Y. Liang *et al.*, nucl-ex/0410027 (2004).
[13] J. J. Aubert *et al.*, Nucl. Phys. **B259**, 189 (1985).
[14] M. Arneodo *et al.*, Nucl. Phys. **B483**, 3 (1997).
[15] I. Abt *et al.*, Nucl. Phys. **B407**, 515 (1993).
[16] T. Ahmed *et al.*, Nucl. Phys. **B439**, 471 (1995).
[17] S. Aid *et al.*, Nucl. Phys. **B470**, 3 (1996).
[18] M. Derrick *et al.*, Z. Phys. **C65**, 379 (1995).
[19] M. Derrick *et al.*, Z. Phys. **C72**, 399 (1996).
[20] V. Tvaskis *et al.*, Phys. Rev. Lett. **98**, 142301 (2007).
[21] A. A. Akhundov, D. Yu. Bardin and N. M. Shumeiko, Sov. J. Nucl. Phys. **26**, 660 (1977); D. Yu. Bardin and N. M. Shumeiko, Sov. J. Nucl. Phys. **29**, 499 (1979); and A. A. Akhundov et al., Sov. J. Nucl. Phys. **44**, 988 (1986).
[22] V. Tvaskis, Ph.D. Thesis, Vrije Universiteit (2004), The Netherlands, unpublished.
[23] L. W. Mo and Y. S. Tsai, Rev. Mod. Phys. **41**, 205 (1969).
[24] M.E. Christy *et al.*, Phys. Rev. C **70**,015206 (2004).
[25] H.P. Blok *et al.*, Phys. Rev. C **78**, 045202 (2008).
[26] The numerical values of all data are available at hallcweb.jlab.org/DISdata.
[27] M. Arneodo *et al.*, Nucl. Phys. **B487**, 3 (1997).
[28] M. Arneodo *et al.*, Nucl. Phys. **B333**, 1 (1989).
[29] A. D. Martin, R. G. Roberts, W. J. Stirling and R. S. Thorne, Phys. Lett. **B604**, 61 (2004).
[30] R. Barbieri, J. R. Ellis, M. K. Gaillard and G. G. Ross, Nucl. Phys. **B117**, 50 (1976).
[31] H. Abramowicz *et al.*, Phys. Lett. **B269**, 465 (1991); H. Abramowicz and A. Levy, hep-ph/9712415 (1997).
[32] D. Gabbert and L. De Nardo, hep-ph/07083196 (2007).
[33] K. Abe *et al.*, Phys. Lett. **B452**, 194 (1999).

TABLE II: Data for the proton and deuteron cross sections and F_2 structure functions as determined via the model-dependent method. The cross sections do not include the virtual-photon flux factor Γ_v (see Eqs. 1,2). Uncertainties are shown without (Δ_{norc}) and with (Δ_{full}) the contribution from radiative corrections.

x	Q^2	ε	σ^p	Δ^p_{norc}	Δ^p_{full}	F_2^p	Δ^p_{norc}	Δ^p_{full}	σ^d	Δ^d_{norc}	Δ^d_{full}	F_2^d	Δ^d_{norc}	Δ^d_{full}
0.009	0.034	0.364	1.0493	0.0689	0.2085	0.0560	0.0072	0.0127	0.9381	0.0411	0.1287	0.0492	0.0060	0.0088
0.009	0.051	0.250	0.4638	0.0409	0.1754	0.0616	0.0094	0.0245	0.4489	0.0240	0.1121	0.0580	0.0082	0.0164
0.009	0.086	0.157	0.2382	0.0242	0.1282	0.0997	0.0166	0.0553	0.2233	0.0138	0.0694	0.0896	0.0137	0.0305
0.015	0.059	0.361	0.4304	0.0241	0.0692	0.0696	0.0082	0.0133	0.4232	0.0155	0.0456	0.0669	0.0077	0.0102
0.015	0.095	0.345	0.2711	0.0144	0.0421	0.0842	0.0093	0.0154	0.2754	0.0096	0.0301	0.0831	0.0091	0.0125
0.015	0.098	0.178	0.2034	0.0190	0.0990	0.0961	0.0150	0.0483	0.2056	0.0111	0.0549	0.0935	0.0133	0.0278
0.015	0.112	0.202	0.1650	0.0144	0.0712	0.0876	0.0128	0.0392	0.1893	0.0090	0.0417	0.0966	0.0130	0.0245
0.015	0.127	0.229	0.1780	0.0123	0.0514	0.1058	0.0137	0.0327	0.1878	0.0077	0.0318	0.1073	0.0134	0.0221
0.015	0.144	0.259	0.1685	0.0099	0.0372	0.1114	0.0131	0.0271	0.1773	0.0066	0.0244	0.1129	0.0131	0.0199
0.015	0.151	0.144	0.0828	0.0079	0.0421	0.1216	0.0186	0.0635	0.0846	0.0047	0.0239	0.1186	0.0166	0.0368
0.015	0.164	0.293	0.1713	0.0085	0.0270	0.1253	0.0133	0.0230	0.1742	0.0058	0.0196	0.1227	0.0131	0.0186
0.015	0.172	0.163	0.0677	0.0062	0.0305	0.1118	0.0163	0.0519	0.0816	0.0039	0.0182	0.1286	0.0169	0.0327
0.025	0.067	0.537	0.8077	0.0278	0.0482	0.0883	0.0070	0.0082	0.7744	0.0198	0.0474	0.0834	0.0066	0.0081
0.025	0.092	0.357	0.2380	0.0106	0.0280	0.0960	0.0101	0.0145	0.2422	0.0074	0.0203	0.0953	0.0101	0.0126
0.025	0.104	0.485	0.4752	0.0164	0.0327	0.1040	0.0084	0.0104	0.4636	0.0120	0.0304	0.0994	0.0082	0.0101
0.025	0.113	0.247	0.1551	0.0090	0.0360	0.1069	0.0133	0.0275	0.1534	0.0058	0.0220	0.1024	0.0125	0.0189
0.025	0.140	0.483	0.3115	0.0099	0.0173	0.1251	0.0094	0.0110	0.3075	0.0075	0.0171	0.1208	0.0093	0.0111
0.025	0.186	0.331	0.1828	0.0072	0.0207	0.1469	0.0138	0.0208	0.1849	0.0052	0.0171	0.1441	0.0138	0.0187
0.025	0.195	0.185	0.0708	0.0048	0.0234	0.1312	0.0166	0.0456	0.0807	0.0032	0.0145	0.1439	0.0173	0.0307
0.025	0.212	0.372	0.1914	0.0066	0.0151	0.1675	0.0141	0.0185	0.1816	0.0047	0.0130	0.1545	0.0134	0.0169
0.025	0.222	0.210	0.0769	0.0042	0.0168	0.1593	0.0181	0.0383	0.0786	0.0028	0.0114	0.1568	0.0176	0.0281
0.025	0.240	0.418	0.1885	0.0058	0.0111	0.1780	0.0133	0.0160	0.1801	0.0044	0.0106	0.1656	0.0128	0.0156
0.025	0.252	0.237	0.0737	0.0034	0.0120	0.1696	0.0175	0.0319	0.0786	0.0024	0.0089	0.1745	0.0181	0.0262
0.025	0.253	0.147	0.0375	0.0028	0.0144	0.1530	0.0198	0.0609	0.0410	0.0018	0.0093	0.1601	0.0193	0.0405
0.025	0.287	0.167	0.0365	0.0023	0.0103	0.1669	0.0197	0.0499	0.0413	0.0016	0.0075	0.1814	0.0204	0.0382
0.040	0.133	0.352	0.1524	0.0055	0.0134	0.1295	0.0125	0.0162	0.1546	0.0041	0.0109	0.1280	0.0126	0.0152
0.040	0.273	0.469	0.2027	0.0053	0.0088	0.2038	0.0133	0.0150	0.1905	0.0041	0.0085	0.1876	0.0126	0.0146
0.040	0.287	0.269	0.0798	0.0031	0.0093	0.2027	0.0190	0.0293	0.0812	0.0022	0.0073	0.2002	0.0190	0.0255
0.040	0.353	0.581	0.2048	0.0046	0.0057	0.2244	0.0107	0.0113	0.1926	0.0038	0.0055	0.2077	0.0103	0.0111
0.040	0.370	0.342	0.0753	0.0022	0.0047	0.2288	0.0173	0.0215	0.0723	0.0018	0.0042	0.2139	0.0166	0.0202
0.040	0.371	0.214	0.0386	0.0016	0.0055	0.2186	0.0209	0.0364	0.0393	0.0012	0.0042	0.2155	0.0206	0.0304
0.040	0.380	0.148	0.0232	0.0013	0.0061	0.2102	0.0230	0.0588	0.0255	0.0009	0.0041	0.2231	0.0235	0.0422
0.040	0.421	0.385	0.0737	0.0020	0.0036	0.2416	0.0162	0.0188	0.0708	0.0016	0.0031	0.2268	0.0157	0.0178
0.060	0.180	0.346	0.1036	0.0032	0.0070	0.1641	0.0148	0.0178	0.1045	0.0025	0.0062	0.1616	0.0149	0.0173
0.060	0.479	0.273	0.0383	0.0012	0.0030	0.2622	0.0203	0.0276	0.0384	0.0009	0.0025	0.2563	0.0202	0.0253
0.060	0.491	0.190	0.0233	0.0009	0.0033	0.2617	0.0234	0.0428	0.0247	0.0007	0.0025	0.2702	0.0240	0.0355
0.060	0.543	0.483	0.0743	0.0017	0.0022	0.2751	0.0138	0.0147	0.0717	0.0014	0.0021	0.2609	0.0135	0.0145
0.060	0.633	0.243	0.0209	0.0006	0.0016	0.2863	0.0205	0.0288	0.0222	0.0005	0.0013	0.2958	0.0212	0.0263
0.080	0.456	0.704	0.2404	0.0044	0.0048	0.2650	0.0086	0.0089	0.2245	0.0038	0.0048	0.2451	0.0081	0.0086
0.080	0.617	0.538	0.0762	0.0015	0.0018	0.2935	0.0124	0.0129	0.0725	0.0013	0.0018	0.2752	0.0119	0.0127
0.080	0.619	0.348	0.0366	0.0009	0.0016	0.2960	0.0179	0.0207	0.0349	0.0008	0.0014	0.2767	0.0170	0.0194
0.080	0.799	0.438	0.0337	0.0007	0.0008	0.3128	0.0135	0.0144	0.0324	0.0006	0.0009	0.2950	0.0131	0.0143
0.080	0.818	0.310	0.0198	0.0005	0.0008	0.3227	0.0171	0.0203	0.0195	0.0004	0.0007	0.3122	0.0167	0.0195
0.125	0.588	0.825	0.2925	0.0047	0.0050	0.2876	0.0061	0.0063	0.2666	0.0041	0.0048	0.2609	0.0055	0.0061
0.125	0.797	0.657	0.0801	0.0014	0.0015	0.3179	0.0089	0.0091	0.0732	0.0012	0.0015	0.2873	0.0082	0.0090
0.125	1.032	0.544	0.0329	0.0006	0.0007	0.3319	0.0097	0.0100	0.0296	0.0005	0.0007	0.2952	0.0087	0.0097
0.125	1.056	0.391	0.0185	0.0004	0.0005	0.3491	0.0131	0.0141	0.0174	0.0003	0.0005	0.3228	0.0122	0.0144
0.175	1.029	0.778	0.0876	0.0013	0.0013	0.3242	0.0060	0.0061	0.0773	0.0011	0.0011	0.2846	0.0052	0.0053
0.175	1.045	0.294	0.0085	0.0002	0.0003	0.3235	0.0142	0.0150	0.0078	0.0002	0.0002	0.2939	0.0129	0.0141
0.175	1.365	0.488	0.0165	0.0003	0.0003	0.3447	0.0109	0.0111	0.0148	0.0003	0.0003	0.3072	0.0099	0.0107
0.250	1.332	0.661	0.0305	0.0005	0.0005	0.3126	0.0074	0.0075	0.0262	0.0004	0.0005	0.2673	0.0065	0.0065
0.250	1.761	0.599	0.0144	0.0002	0.0002	0.3183	0.0082	0.0083	0.0125	0.0002	0.0002	0.2744	0.0071	0.0071
0.450	2.275	0.715	0.0099	0.0002	0.0002	0.2104	0.0046	0.0046	0.0077	0.0001	0.0001	0.1638	0.0036	0.0036

TABLE III: Ratio of deuteron to proton cross sections and structure functions. Uncertainties are shown without (Δ_{noa2}) and with (Δ_{full}) the contribution from radiative corrections of order α^2.

x	Q^2	ε	σ^d/σ^p	Δ_{noa2}	Δ_{full}	F_2^d/F_2^p	Δ_{noa2}	Δ_{full}
0.0080	0.0332	0.3521	0.8952	0.0540	0.0758	0.8798	0.0562	0.0774
0.0080	0.0509	0.2500	0.9426	0.0682	0.1339	0.9170	0.0728	0.1363
0.0080	0.0883	0.1605	0.8812	0.0719	0.1587	0.8448	0.0806	0.1628
0.0125	0.0359	0.3791	0.8513	0.0495	0.0633	0.8367	0.0516	0.0649
0.0125	0.1092	0.1977	1.0555	0.0644	0.1558	1.0129	0.0773	0.1616
0.0175	0.0593	0.3692	0.9613	0.0358	0.0418	0.9413	0.0410	0.0464
0.0175	0.0977	0.3247	1.0040	0.0373	0.0499	0.9766	0.0463	0.0569
0.0175	0.1553	0.2186	1.0137	0.0365	0.0598	0.9768	0.0519	0.0703
0.0250	0.0677	0.5390	0.9600	0.0298	0.0330	0.9452	0.0333	0.0361
0.0250	0.1085	0.3985	0.9840	0.0258	0.0282	0.9621	0.0338	0.0357
0.0250	0.2285	0.2567	0.9832	0.0247	0.0272	0.9529	0.0389	0.0405
0.0350	0.1022	0.5321	0.9646	0.0260	0.0274	0.9484	0.0306	0.0318
0.0350	0.1362	0.4030	0.9909	0.0254	0.0276	0.9689	0.0335	0.0352
0.0350	0.1765	0.2981	0.9942	0.0302	0.0408	0.9656	0.0416	0.0498
0.0350	0.3099	0.2974	0.9612	0.0221	0.0232	0.9375	0.0322	0.0329
0.0500	0.1713	0.5122	0.9732	0.0210	0.0210	0.9593	0.0251	0.0252
0.0500	0.3712	0.4090	0.9445	0.0199	0.0200	0.9273	0.0262	0.0262
0.0500	0.4644	0.2699	0.9897	0.0222	0.0232	0.9651	0.0330	0.0337
0.0700	0.2195	0.5146	0.9299	0.0213	0.0216	0.9140	0.0266	0.0268
0.0700	0.2692	0.4810	0.9576	0.0198	0.0199	0.9426	0.0247	0.0247
0.0700	0.4464	0.6947	0.9341	0.0193	0.0193	0.9253	0.0212	0.0212
0.0700	0.5624	0.4355	0.9641	0.0208	0.0210	0.9474	0.0267	0.0268
0.0700	0.6390	0.2965	0.9894	0.0225	0.0234	0.9670	0.0316	0.0323
0.0900	0.2936	0.4363	0.9530	0.0197	0.0197	0.9361	0.0259	0.0259
0.0900	0.4998	0.4794	0.9419	0.0187	0.0187	0.9310	0.0215	0.0215
0.0900	0.6328	0.5494	0.9384	0.0200	0.0200	0.9256	0.0238	0.0238
0.0900	0.7947	0.3526	0.9627	0.0212	0.0214	0.9436	0.0285	0.0286
0.1100	0.5649	0.8075	0.9197	0.0183	0.0183	0.9147	0.0190	0.0190
0.1100	0.8072	0.5470	0.9274	0.0187	0.0187	0.9162	0.0217	0.0217
0.1100	1.0138	0.4026	0.9491	0.0211	0.0211	0.9324	0.0269	0.0269
0.1400	0.4647	0.6166	0.9187	0.0182	0.0182	0.9099	0.0202	0.0202
0.1400	0.6204	0.8495	0.9080	0.0187	0.0187	0.9045	0.0190	0.0190
0.1400	0.8409	0.6831	0.9045	0.0191	0.0191	0.8967	0.0206	0.0206
0.1400	1.0623	0.5063	0.8971	0.0181	0.0181	0.8850	0.0218	0.0218
0.1800	0.5036	0.6698	0.9202	0.0183	0.0183	0.9136	0.0194	0.0194
0.1800	0.7065	0.9009	0.8918	0.0189	0.0189	0.8901	0.0190	0.0190
0.1800	0.9981	0.5371	0.8861	0.0176	0.0176	0.8802	0.0185	0.0185
0.1800	1.3393	0.5233	0.8947	0.0179	0.0179	0.8853	0.0202	0.0202
0.2250	0.7407	0.9170	0.8775	0.0173	0.0173	0.8765	0.0173	0.0173
0.2250	1.0817	0.5354	0.8625	0.0171	0.0171	0.8583	0.0176	0.0176
0.2250	1.3655	0.6727	0.8743	0.0177	0.0177	0.8700	0.0182	0.0182
0.2250	1.6733	0.5761	0.8817	0.0180	0.0180	0.8775	0.0185	0.0185
0.2750	0.7749	0.9313	0.8371	0.0176	0.0176	0.8367	0.0176	0.0176
0.2750	1.2362	0.8579	0.8305	0.0171	0.0171	0.8303	0.0171	0.0171
0.2750	1.7101	0.5221	0.8667	0.0169	0.0169	0.8653	0.0170	0.0170
0.3500	1.3006	0.5544	0.8340	0.0153	0.0153	0.8340	0.0153	0.0153
0.3500	1.7109	0.5575	0.8279	0.0153	0.0153	0.8279	0.0153	0.0153
0.3500	2.1840	0.6967	0.8243	0.0167	0.0167	0.8243	0.0167	0.0167
0.4500	2.3660	0.7325	0.7881	0.0144	0.0144	0.7881	0.0144	0.0144